Supplemental information

Ephexin1 is required for structural maturation and neurotransmission at the neuromuscular junction

Lei Shi, Busma Butt, Fanny C.F. Ip, Ying Dai, Liwen Jiang, Wing-Ho Yung, Michael E. Greenberg, Amy K.Y. Fu and Nancy Y. Ip

Supplemental figures

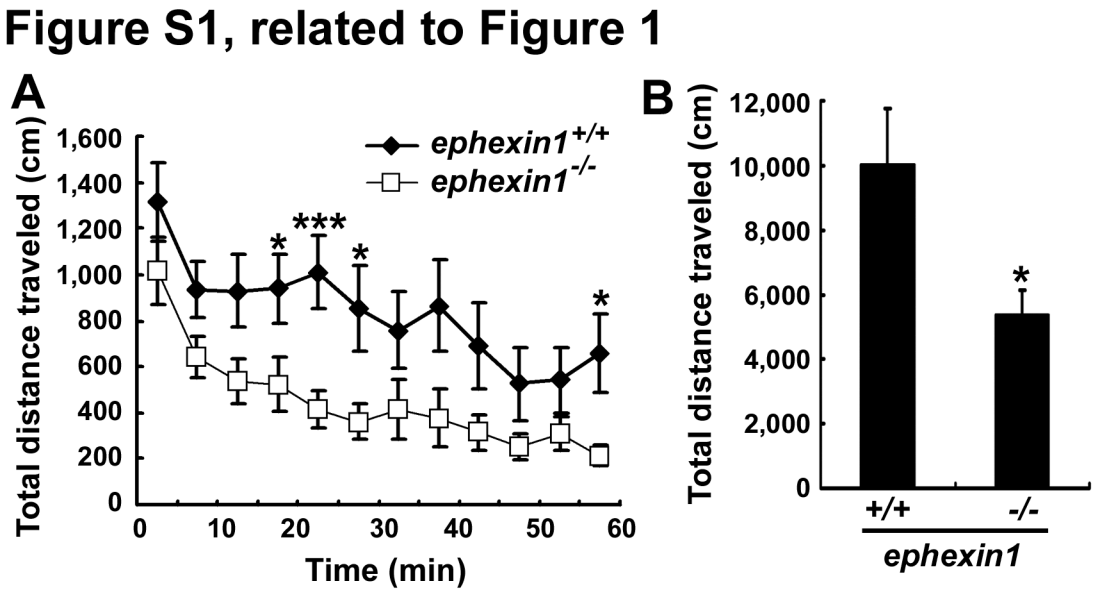

Figure S1 ***ephexin1*$^{-/-}$ mice exhibited reduced spontaneous motor activity in the open field test.** The distance traveled in every 5 min (A) and total distance traveled over 60 min (B) were determined in wild type (n = 17) and *ephexin1*$^{-/-}$ mice (n = 14). Mean ± SEM, *p <0.05, ***p <0.005; Student's *t*-test.

Figure S2, related to Figure 2

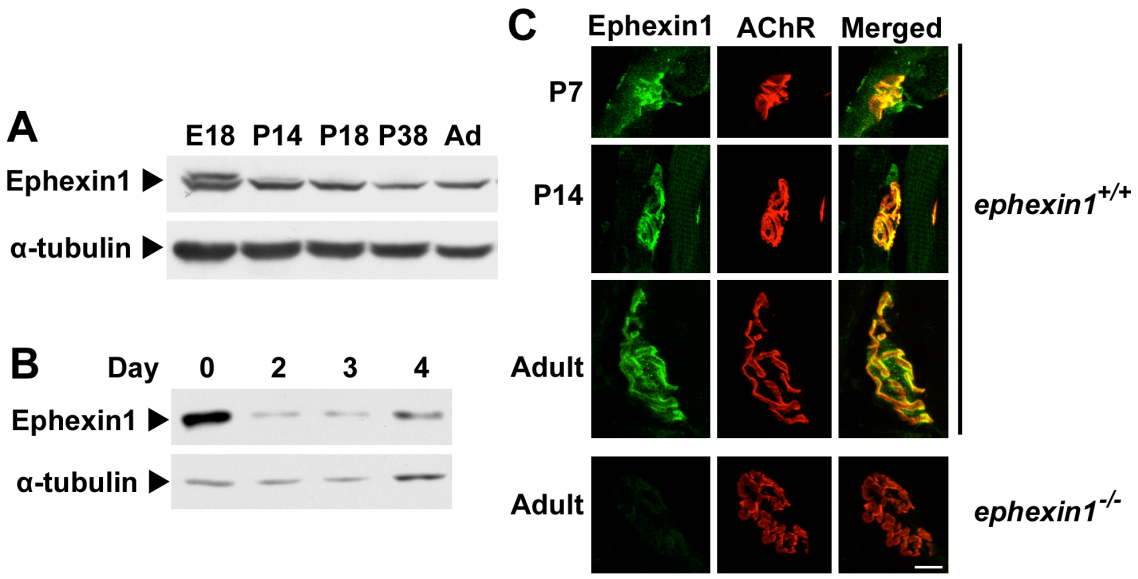

Figure S2 **Expression of ephexin1 in muscle.** Ephexin1 protein is expressed in mouse skeletal muscle (A) and in cultured C2C12 myotubes (B). Lysates from mouse gastrocnemius muscle at indicated stages (E18-adult) (A) or from cultured C2C12 myotubes upon differentiation (B) were subjected to Western blot analysis for ephexin1. α-tubulin served as a loading control. (C) Ephexin1 protein becomes concentrated at the adult NMJ. Longitudinal sections of mouse sternomastoid muscle at P7, P14 and adult were co-stained with ephexin1 antibody (green) and α-BTX (red). The immunoreactivity for ephexin1 was not detected at NMJs of adult *ephexin1*$^{-/-}$ mice, indicating that the staining for ephexin1 was specific.

Figure S3, related to Figure 3

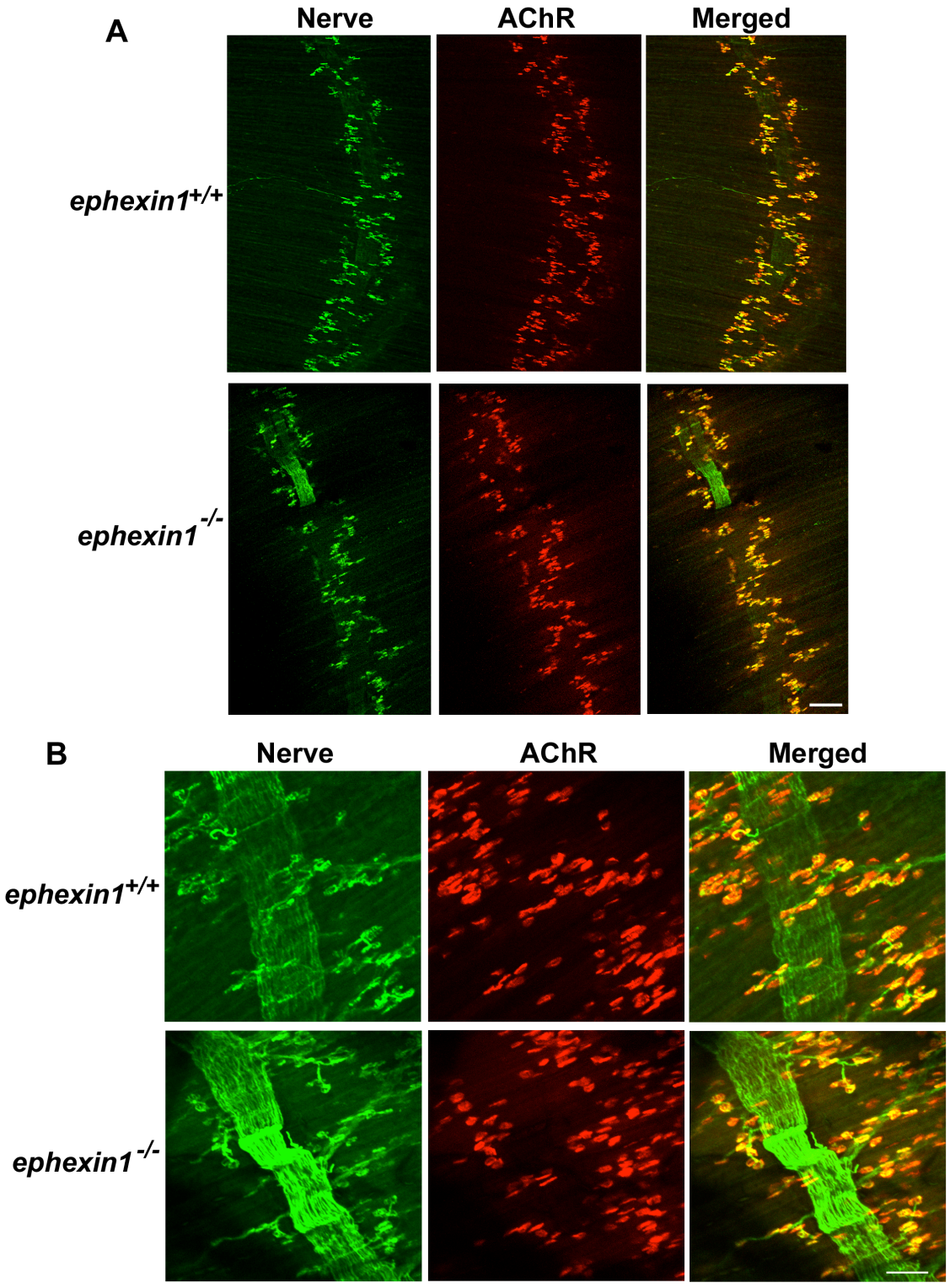

Figure S3 The morphology of NMJs in *ephexin1*$^{-/-}$ mice is grossly normal at birth. (A) Whole-mount diaphragms of P2 wild type and *ephexin1*$^{-/-}$ mice were co-stained with anti-synaptophysin and neurofilament antibodies for presynaptic axon terminals (green) and α-BTX for postsynaptic AChR clusters (red). Scale bar, 100 μm. (B) A higher magnification showing the nerve and AChR staining. No obvious morphological defects were found in either the motor nerve terminals or postsynaptic AChRs clusters. Scale bar, 50 μm.

Figure S4, related to Figure 4

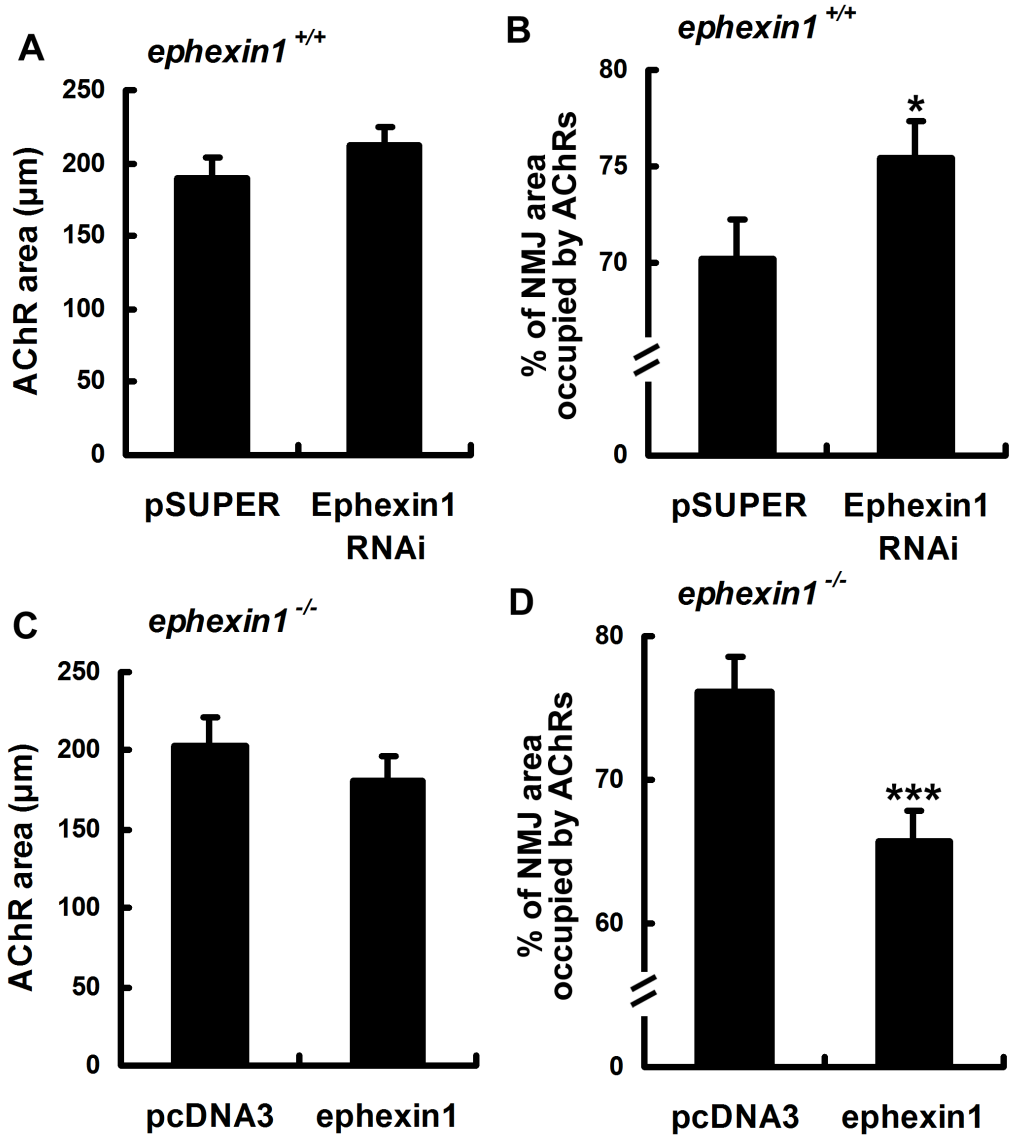

Figure S4 Muscle ephexin1 regulates postnatal disassembly of AChR clusters. (A and B) Knockdown of ephexin1 in muscle results in enlarged AChR area (A) and increased synaptic area occupied by AChRs (B). (n = 23 from 7 mice injected with pSUPER vector; n = 20 from 8 mice injected with ephexin1 shRNA). (C and D) Overexpression of ephexin1 in *ephexin1*$^{-/-}$ muscles restored the plaque-pretzel transition of AChR clusters to normal. Quantification of AChR area (C) and NMJ area occupied by AChRs (D). (n = 11 from 5 pcDNA3-injected mice; n = 17 from 5 ephexin1-injected mice.). Mean ± SEM, *p <0.05, ***p <0.005, Student's *t*-test.

Figure S5, related to Figure 6

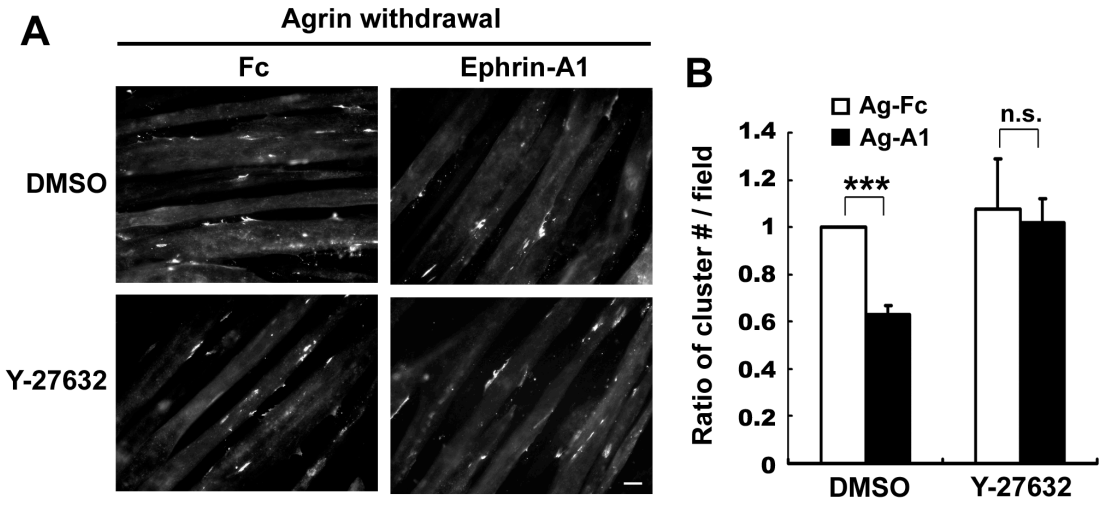

Figure S5 Blockade of RhoA-mediated signaling inhibits ephrin-A1-induced AChR cluster dispersal. Myotubes were first treated with agrin to induce AChR clustering. Immediately after the withdrawal of agrin, myotubes were pre-treated with the ROCK inhibitor Y-27632 (10 μM) for 30 min, and then subjected to ephrin-A1 treatment with the presence of Y-27632 for 12-14 hr. Data are represented as a ratio of AChR cluster number. Mean ± SEM of at least three experiments (***p <0.005, ephrin-A1 versus Fc in DMSO-treated myotubes; n.s., p >0.05, ephrin-A1 versus Fc in myotubes co-treated with Y-27632, Student's *t*-test).

Figure S6, related to Figure 3 and discussion

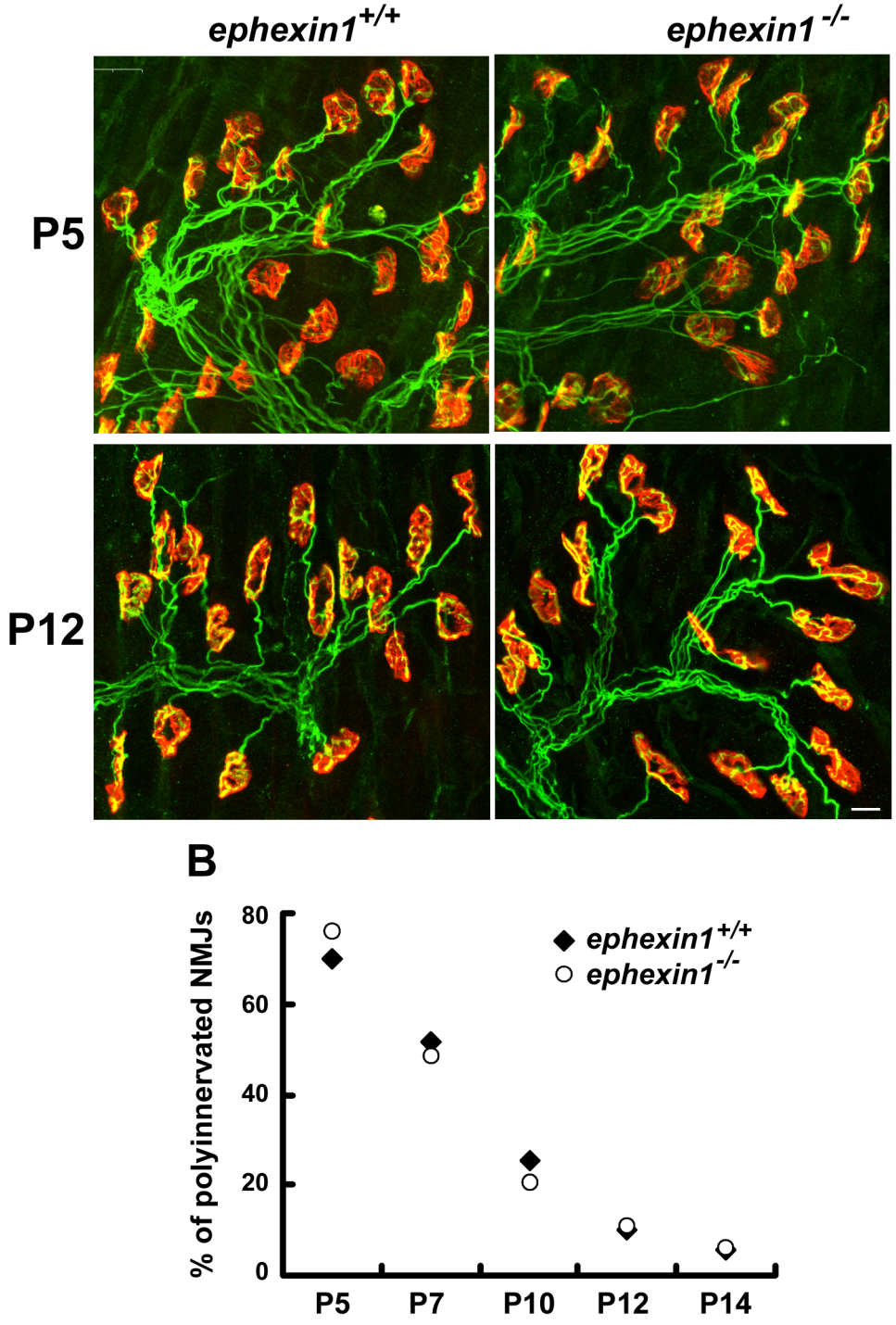

Figure S6 Synapse elimination in *ephexin1*$^{-/-}$ mice is apparently normal. (A) Individually teased tibialis anterior muscle fibers of P5 and P12 *ephexin1*$^{-/-}$ and their

corresponding wild type littermates were co-stained with anti-synaptophysin and neurofilament antibodies for presynaptic motor nerve terminals (green) and α-BTX for postsynaptic AChR clusters (red). (B) Quantification analysis of the percentage of NMJs that are innervated by more than one axon (polyinnervated). n ≥ 87 from 3 *ephexin1*$^{-/-}$ or *ephexin1*$^{+/+}$ mice at each stage.

Figure S7, related to Figure 6 and discussion

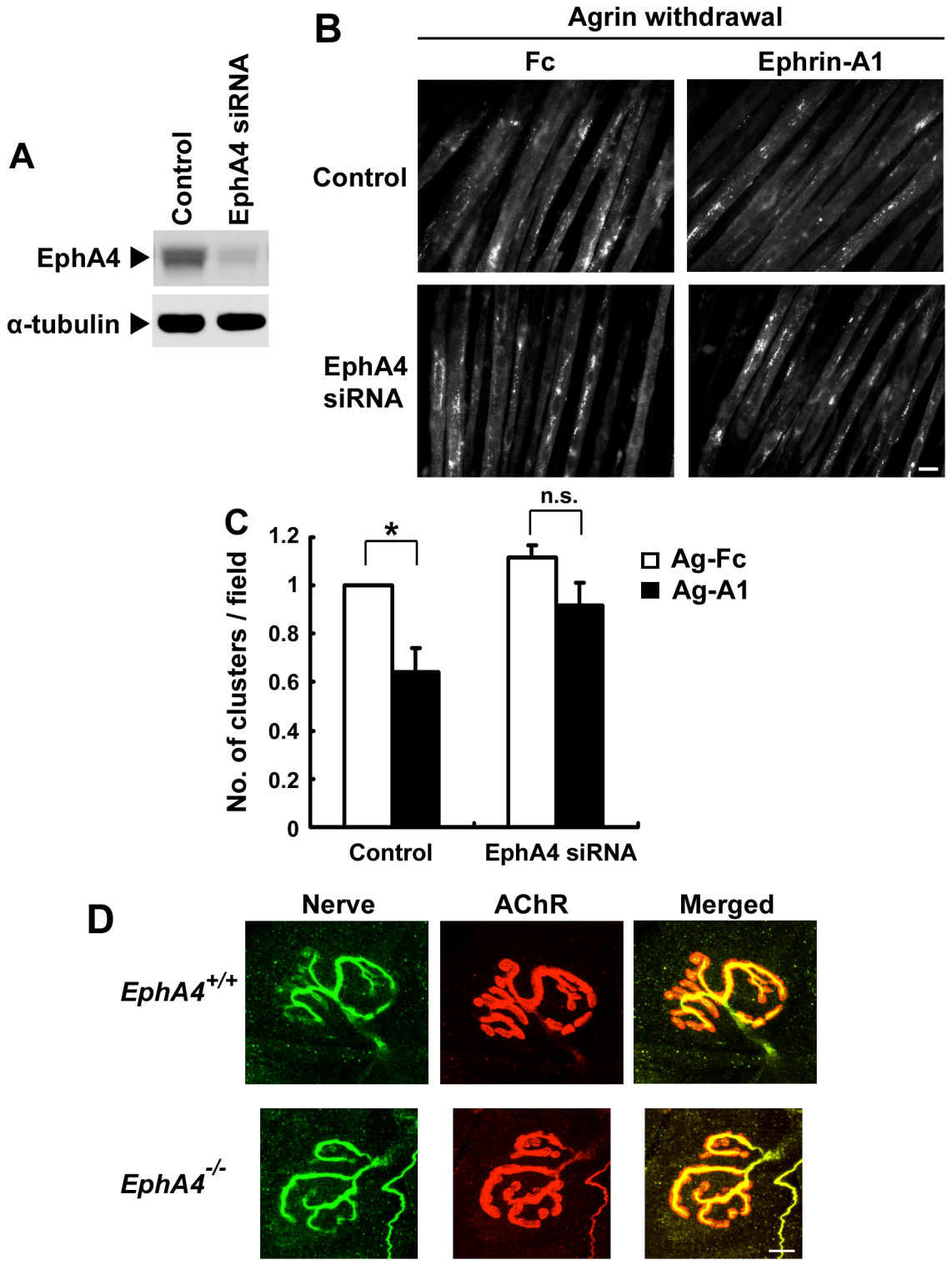

Figure S7 EphA4 regulates the dispersal of AChR clusters in cultured myotubes. (A) Knockdown of EphA4 in C2C12 myotubes by EphA4 siRNA. α-tubulin acts as a control for equal protein loading. (B and C) Knockdown of EphA4 in myotubes abolished the ephrin-A1-induced dispersal of pre-existing AChR clusters. Myotubes expressing ephexin1-siRNA were first treated with agrin to induce AChR clustering. Following agrin withdrawal, myotubes were treated with ephrin-A1 or Fc control for 12-14 hr. Scale bar, 20 μm. (C) Data were presented as a ratio of AChR cluster number / field. Mean ± SEM of at least three experiments. *p <0.05, ephrin-A1 versus Fc in control myotubes; n.s. = not significant, p >0.05, ephrin-A1 versus Fc in EphA4 knockdown myotubes, Student's *t*-test. (D) Adult *EphA4*$^{-/-}$ NMJs do not exhibit gross abnormalities. Individually teased sternomastoid muscle fibers of adult *EphA4*$^{-/-}$ mice and their corresponding wild type littermates were double-stained with anti-synaptophysin and neurofilament antibodies for presynaptic axon terminals (Nerve; green) and α-BTX for postsynaptic AChR clusters (red). *EphA4*$^{-/-}$ NMJs showed mature pretzel-shaped AChRs and precise synaptic apposition, which were similar to the phenotype of *EphA4*$^{+/+}$ NMJs. Scale bar, 10 μm.

Table S1 **Microscopic analysis of NMJs in *ephexin1* $^{+/+}$ and *ephexin1* $^{-/-}$ mice. (related to Figure 3)**

Age of mice		P2	P5	P10-11	P14	P17-18	P38	Adult[1]
AChR area (μm^2)	*ephexin1* $^{+/+}$	80.8±4.6[2] (n=65)	84.1±3.4 (n=43)	136.6±3.8 (n=176)	161.4±6.3 (n=63)	146.6±5.4 (n=71)	296.8±16.6 (n=23)	373.7±15.6 (n=82)
	ephexin1 $^{-/-}$	71.6±5.2 (n=41)	97.9±4.3 (n=93)	156.6±5.3 (n=173)	189.6±7.1 (n=76)	196.3±6.8 (n=97)	271.3±11.7 (n=29)	342.3±10.8 (n=83)
	p value	>0.05[3]	*<0.05	***<0.005	***<0.005	***<0.005	>0.05	>0.05
NMJ area (μm^2)	*ephexin1* $^{+/+}$	80.8±4.6 (n=65)	84.1±3.4 (n=43)	148.9±4.3 (n=176)	197.6±9.9 (n=63)	178.0±7.3 (n=71)	518.2±34.8 (n=23)	962.7±49.5 (n=84)
	ephexin1 $^{-/-}$	71.6±5.2 (n=41)	97.9±4.3 (n=93)	172.3±6.5 (n=173)	226.6±9.8 (n=76)	223.9±9.1 (n=97)	471.4±25.8 (n=29)	1015.0±38.0 (n=87)
	p value	>0.05	*<0.05	***<0.005	*<0.05	***<0.005	>0.05	>0.05
% of NMJ occupied by AChR	*ephexin1* $^{+/+}$	100 (n=65)	100 (n=43)	92.7±0.9 (n=176)	84.4±1.3 (n=63)	84.0±1.1 (n=71)	58.7±1.6 (n=23)	40.4±0.8 (n=82)
	ephexin1 $^{-/-}$	100 (n=41)	100 (n=93)	93.3±0.6 (n=173)	85.9±1.1 (n=76)	89.8±0.9 (n=97)	59.5±1.8 (n=29)	35.9±0.8 (n=83)
	p value	N/A	N/A	>0.05	>0.05	***<0.005	>0.05	***<0.005
% of NMJ with perforated AChR	*ephexin1* $^{+/+}$		9.9 (n=181)	54.0 (n=213)	80.0 (n=150)	97.2 (n=110)		
	ephexin1 $^{-/-}$		10.3 (n=78)	43.6 (n=236)	66.2 (n=139)	84.9 (n=100)		

		P5	P7	P10	P12	P14
% of polyinnervated NMJ	*ephexin1* $^{+/+}$	70.5 (n=149)	51.7 (n=87)	25.6 (n=137)	10.0 (n=90)	5.6 (n=90)
	ephexin1 $^{-/-}$	76.1 (n=117)	48.3 (n=89)	20.5 (n=156)	10.8 (n=93)	5.9 (n=101)

1. Results of P2 to P38 mice are from whole mount preparations of tibialis anterior muscle, while results of adult mice are from whole mount preparations of sternomastoid muscle.

2. All values are reported as mean ± SEM (n is the number of NMJs measured), at least 3 wild type or mutant mice at each stage are examined.

3. All the p values are generated using Student's t-test.

Table S2 AChR area in *ephexin1*$^{+/+}$ and *ephexin1*$^{-/-}$ mice (P5-P9) (Related to Figure 3)

		P5	P7	P9[1]
AChR area (μm^2)	***ephexin1*$^{+/+}$**	109.0±4.9[2] (n=99)	93.0±4.4 (n=71)	96.5±5.5 (n=88)
	***ephexin1*$^{-/-}$**	104.7±4.5 (n=113)	106.7±5.9 (n=84)	148.4±9.2 (n=82)
	p value	>0.05[3]	=0.06	***<0.005

1. Results are obtained from whole mount preparations of sternomastoid muscle

2. All values are reported as mean ± SEM (n is the number of NMJs measured), at least 3 wild type or mutant mice at each stage are examined.

3. All the p values are generated using Student's t-test.

Supplemental experimental procedures

Constructs and chemicals

pSUPER ephexin1 shRNA was prepared as previously described (Fu et al., 2007). Chemically synthesized siRNA (small interfering RNA) targeting ephexin1 was designed and synthesized according to the manufacturer's instruction using Stealth RNAi technology (Invitrogen). The oligonucleotide sequences specific for mouse ephexin1 is GGACCAAGUUUGTAUCCUU, and the sequence for corresponding scramble control siRNA is GGUUCCAUCUAGUAUACGU. The oligonucleotide sequences specific for mouse EphA4 is GGCGCAGAGGGUGUACAUUGAAAUU, and the sequence for corresponding scramble control siRNA is GGCGAGAGGGUAUACUUAGACGAUU. The mRNAs encoding for GFP, GFP-RhoA-CA, ephexin1, and its mutant (Y87F) were *in vitro* transcribed from corresponding expression plasmids using mMESSAGE mMACHINE® T7 Ultra Kit (Ambion). Y-27632 was purchased from Sigma.

Open field test

For open field test, the mice were first placed in the center of an open activity box (50 X 50 X 40 cm) for 1 hr for them to become familiar with the environment. The spontaneous activity of these mice in the open field was then recorded for 60 min using EthoVision XT software (Noldus Information Technology BV, The Netherlands). Distance at 5 min-interval and total distance traveled by the mice were measured.

Immunohistochemical analysis for ephexin1 localization at the NMJ

To examine the localization of ephexin1 at the NMJ, mouse sternomastoid muscles from different stages were dissected and fixed in 1% formaldehyde at 4^{o}C overnight (Fu et al., 1999). Muscle cryosections (20 μm) were prepared and incubated with 0.1 M glycine in PBS, and permeabilized with 0.5% Triton X-100/PBS for 20 min. The sections were then blocked and incubated with antibody against ephexin1 in PBS with 5% BSA

and 10% FBS, followed by washing and incubation with FITC-conjugated goat anti-rabbit antibody and α-BTX. The muscle sections were washed and mounted in Mowiol (Calbiochem). Z-serial images of ~5 layers (1 μm for each layer) were collected with confocal microscopy (63X magnification; BX61, Olympus, Japan). The images presented represent single-plane projections derived from overlaying each set of Z-images.

RhoA activation assay

RhoA GTPase activity was measured using pull-down analysis as described (Fu et al., 2007). Briefly, lysates of C2C12 myotubes were collected and active RhoA was pull-down by incubation with GST-RBD, a Rhotekin domain that specifically binds to the GTP-bound form of RhoA. The level of active RhoA was subsequently measured using Western blot analysis.

Reference

Fu, A. K., Smith, F. D., Zhou, H., Chu, A. H., Tsim, K. W., Peng, B. H., and Ip, N. Y. (1999). Xenopus muscle-specific kinase: molecular cloning and prominent expression in neural tissues during early embryonic development. Eur J Neurosci *11*, 373-382.

Fu, W. Y., Chen, Y., Sahin, M., Zhao, X. S., Shi, L., Bikoff, J. B., Lai, K. O., Yung, W. H., Fu, A. K., Greenberg, M. E., and Ip, N. Y. (2007). Cdk5 regulates EphA4-mediated dendritic spine retraction through an ephexin1-dependent mechanism. Nat Neurosci *10*, 67-76.